ROM SAF Report 27
Ref: SAF/ROM/METO/REP/RSR/027
Web: www.romsaf.org
Date: 11 November 2016

The EUMETSAT Network of Satellite Application Facilities

ROM SAF
Radio Occultation Meteorology

ROM SAF Report 27

Recent forecast impact experiments with GPS radio occultation measurements

Sean Healy

ECMWF

Document Author Table

	Name	Function	Date	Comments
Prepared by:	S. Healy	ROM SAF Project Team	11 November 2016	
Reviewed by:	C. Burrows	ROM SAF Project Team	9 November 2016	
Reviewed by:	-	-	-	
Approved by:	K. B. Lauritsen	ROM SAF Project Manager	11 November 2016	

Document Change Record

Issue/Revision	Date	By	Description
1.0	11 November, 2016	S. Healy	

ROM SAF

The Radio Occultation Meteorology Satellite Application Facility (ROM SAF) is a decentralised processing centre under EUMETSAT which is responsible for operational processing of GRAS radio occultation data from the Metop satellites and RO data from other missions. The ROM SAF delivers bending angle, refractivity, temperature, pressure, and humidity profiles in near-real time and offline for NWP and climate users. The offline profiles are further processed into climate products consisting of gridded monthly zonal means of bending angle, refractivity, temperature, humidity, and geopotential heights together with error descriptions.

The ROM SAF also maintains the Radio Occultation Processing Package (ROPP) which contains software modules that will aid users wishing to process, quality-control and assimilate radio occultation data from any radio occultation mission into NWP and other models.

The ROM SAF Leading Entity is the Danish Meteorological Institute (DMI), with Cooperating Entities: i) European Centre for Medium-Range Weather Forecasts (ECMWF) in Reading, United Kingdom, ii) Institut D'Estudis Espacials de Catalunya (IEEC) in Barcelona, Spain, and iii) Met Office in Exeter, United Kingdom. To get access to our products or to read more about the project please go to: http://www.romsaf.org

Intellectual Property Rights

Abstract

The results from a recent set of forecast impact experiments with GPS radio occultation (GPS-RO) measurements are summarised. Although the main impact of GPS-RO is in the upper-troposphere and stratosphere, it is shown that the data has some positive impact on tropospheric humidity and winds, particularly in the southern hemisphere. Spatial maps of GPS-RO bending angle departure statistics for the lowest 2 km are presented, and it is suggested that some bias features may be related to ECMWF humidity forecast bias, rather than just observation or forward model errors. The GPS-RO impact does not appear to be sensitive to increasing and reducing the assumed errors statistics in the troposphere, but increasing the assumed errors statistics in the stratosphere does have a positive impact. The relevance of these results to ongoing ROM SAF activities is discussed.

Contents

1 Background and Main Results

1.1 Introduction

Assimilation experiments with the ECMWF numerical weather prediction (NWP) system can provide useful information for the ROM SAF. This is because ECMWF short-range forecasts are used in the operational ROM SAF one-dimensional variational (1D-Var) retrieval, and ECMWF also uses the bending angle observation operators provided in the Radio Occultation Processing Package (ROPP) (Culverwell *et al.* 2015). In addition, there will be increasing interest in the tropospheric impact of GPS-RO measurements within the ROM SAF, now that Metop GRAS measurements are processed with wave optics techniques and can be used down to the surface.

This report summarises recent assimilation experiments with GPS-RO measurements, highlighting the potential relevance of the results to the ROM SAF products. Note that the experiments related to the retrieval of surface pressure information from GPS-RO are given in Healy (2013). The impact of GPS-RO on tropospheric and stratospheric temperature, humidity and vector wind forecast scores is presented. The largest impact is in the upper troposphere and lower/middle stratosphere as expected, but we see some improvement in the relative humidity forecasts in the troposphere, particularly in the southern hemisphere. It is also shown that assimilating GPS-RO improves the fit to both ATMS temperature and tropospheric humidity channels, radiosonde temperatures and, most surprisingly, wind measurements in the tropics. Spatial maps of bending angle biases in the lower troposphere are presented, illustrating that the situation is more complex than a simple negative observation bias in the troposphere, and that model deficiencies may also have to be considered in this context. The impact of a two-dimensional bending angle operator is assessed, and we present the sensitivity of the forecast impact scores to both doubling and halving the assumed bending angle error statistics in the troposphere. Increasing the assumed GPS-RO errors in the stratosphere is also presented, because this change is now operational at ECMWF.

Section 1.2 describes the experiments that have been performed. The main results are given in section 1.3, and the summary and conclusions are in section 2.

1.2 Forecast impact Experiments

The experiments cover the period December 1, 2014 to February 28, 2015, and are performed at T511 resolution, giving a horizontal sampling of $\sim$ 38 km. By default the GPS-RO data are assimilated with the two-dimensional bending angle operator used operationally at ECMWF, but some tests with a one-dimensional operator are also included. Unless stated otherwise, the assumed error covariance matrix, $\mathbf{R}$, used to assimilate the GNSS-RO data is a global model, and vertical error correlations are not included. The percentage bending

angle errors are given as a function of impact height, h, which is defined as impact parameter minus radius of curvature $(a - r_c)$. They fall linearly from 20 % at h=0 to 1% at h=10 km. The errors above 10 km are then 1% until this reaches a lower absolute limit of 3 microradians.

The following experiments have been performed:

1. **CTL**: The control experiment, assimilating all the data used operationally for the period, including assimilating GPS-RO with a 2D operator.
2. **NoRO**: As the control, but GPS-RO measurements are removed.
3. **1D**: As the control, but the GPS-RO data assimilated with a 1D operator.
4. **HIWT**: Increasing the weight given to GPS-RO in the troposphere by assuming the bending angle uncertainty falls linearly from from 10 % at h=0 to 1% at h=10 km.
5. **LOWT**: Reducing the weight given to GPS-RO in the troposphere by assuming the bending angle uncertainty falls linearly from from 40 % at h=0 to 1% at h=10 km.
6. **43R1**: A more recent ECMWF configuration. Reducing the weight given to GPS-RO in the stratosphere by increasing the bending angle uncertainty from 1 % to 1.25 % above impact heights of 10 km. Tightening the first guess quality control by rejecting bending angles if the magnitude of the departure is greater than 6.25 $\times\sigma_o$. This threshold is currently $\sim$ 11 $\times\sigma_o$.

1.3 Main results

In general, the verification of the forecasts are performed against “own analyses” and statistical significance estimates are included at the 95 % level, using the ECMWF IVER package (Geer, 2015). The improvements of the short-range (12 hour) forecast fit to observations are also presented.

Impact of GPS-RO

Comparing the CTL and NoRO experiments highlights where the GPS-RO impact is currently largest, and where possible improvements can be made. Figures 1.1, 1.2 and 1.3 show the fractional improvement in the standard deviation of the forecast errors for temperature, relative humidity and vector winds, respectively, when comparing the CTL and NoRO experiments. Values below the zero line indicate that the GPS-RO measurements have reduced the standard deviation of the forecast errors. Similar results are found for the anomaly correlation and root-mean-square statistics, but they will not be shown here. As is often the case with satellite data, the impact of GPS-RO is larger in the southern hemisphere than in the northern hemisphere, because of the larger number of conventional data in the northern hemisphere. The impact on the temperature forecasts at 850 hPa and 500 hPa is clear in the southern hemisphere, and the improvement at 500 hPa is statistically significant up to day-7. There is a general reduction in the humidity errors at 1000, 500 and 850 hPa, and it is statistically significant at 500 hPa for days 2,3 and 4, and at day-4 for 1000 hPa. The vector wind scores also show some statistical significance at 1000, 850 and 500 hPa. There is some improvement in the temperature and relative humidity errors statistics in the tropics

at 850 hPa, and the improvements appear to be statistically significant at day-3 and day-4. The results in the northern hemisphere are generally neutral in the troposphere.

The results above 200 hPa appear to be problematic because they indicate that the GPS-RO measurements are increasing the forecast errors errors in the short-range. The GPS-RO "core region", where the measurements have their greatest information content, is usually considered to be in the interval between $\sim$ 200 hPa to around 5 hPa. This apparent contradiction is a well known verification issue, related to using "own" analyses. Comparing against other observation types in the short-range is considered more reliable. Figures 1.4 and 1.5 show globally averaged, vertical profiles of the normalised departure statistics for radisonde temperature and radisonde, pilot and a profiler vector winds. More precisely, the standard deviation of the observation minus background or "first guess" (o-b) and observation minus analysis (o-a) departures are computed for both experiments, and then the CTL standard deviation divided by NoRO standard deviation values are plotted as a percentage. Therefore, 100 % indicates that the CTL and NoRO departures have the same standard deviation values. Values below 100 % indicate that the GPS-RO measurements used in the CTL experiment are improving the fit to the other observations, and there is a positive impact on the short-range forecasts for both temperature and vector wind in the upper troposphere and stratosphere. The impact on the temperature statistics in the upper troposphere and stratosphere is very large compared to other observation types – particularly in the southern hemisphere – but this is to be expected and has been noted a number of times. The worsening of the analysis departures is not considered problematic, if the short-range forecasts are improved. The GPS-RO bending angle forward operator does not increment winds directly, so the wind information must be coming from the integration of the NWP model as part of the 4D-Var assimilation, and through correlations in the background error covariance matrix. We note that the improvements in wind includes a strong signal the tropical region, with a $\sim$ 2 % reduction in the background departures above 100 hPa (Figure 1.6). This improvement in the tropical winds appears to be mainly driven by the GPS-RO measurements assimilated in the latitude band between $\pm 20^{o}$, and it is of similar magnitude to the improvement in the standard deviation of tropical radiosonde temperature (o-b) departures (Figure not shown). The mechanism leading to this improvement is not clear at present, and requires further investigation. The kink in Figure 1.5 around 70 hPa is apparent in both the northern and southern hemisphere extra-tropics, but not in the tropics. It may be related to incorrect correlations in the background error covariance matrix.

In general, the assimilation of GPS-RO measurements improves the short-range forecast departure statistics for other satellite data. For example, Figure 1.7 shows the globally averaged fit to ATMS radiances. Channels 18-22 relate to humidity information and peak in the troposphere, and channels 6-15 provide temperature information from the troposphere to stratosphere, with the channel 6 weighting function peaking lowest near 700 hPa (See Figure 1, Bormann *et al.*, (2013) for the ATMS weighting functions). It is clear that the GPS-RO data is providing a statistically significant improvement in the fit to both the ATMS temperature and humidity channels, which is encouraging. Similar improvements are also found for AMSU-A departures, with the exception of channel 8 which shows a small degradation. This may be a result of GPS-RO adding vertical structure around the tropopause.

Spatial maps of the mean bending angle departures are shown in Figure 1.8 and Figure 1.9, for the 2-3 km and 3-4 km impact height intervals, respectively. These are computed for the full 3 months of the experiment. GPS-RO retrievals are known to have a negative

refractivity bias in the tropical lower troposphere (Ao *et al.*, 2003), but the bending angle bias patterns are complex in lowest two kilometers, and they may also be related in part to NWP model deficiencies. These biases are quite large, and are comparable to the assumed GPS-RO error standard deviations used when assimilating the data. We see similar results with the current ECMWF operational forecasts for a more recent period, and it is interesting to note that the corresponding plots from the Met Office have quite different bias characteristics (Chris Burrows Met Office, personal communication). In Figure 1.8 we see both positive and negative biases. The largest negative biases are in regions of strong convection associated with the intertropical convergence zone (ITCZ), and where the NWP total column water values are also largest (Figure not shown). The largest positive biases are to the west of the major continents (e.g, to the west of Chile). These are regions of semi-permanent marine stratocumulus sheets, related to large scale descent, and they are characterised by very large refractivity gradients at the top of the planetary boundary layer. In the 3-4 km interval, shown in Figure 1.9, we see primarily positive bending angle biases over the oceans, with weaker negative biases only apparent around the ITCZ.

In the ECMWF operational system, there was a change in the bending angle biases in the tropics after the introduction of a maximum refractivity gradient in the ROM SAF bending angle forward models. The maximum gradient is now (-)0.75 N units m^{-1}, and this was introduced into both the ROM SAF 1D and 2D operators to constrain the magnitude of the simulated bending angle gradients with respect to model humidity ($\partial\alpha/\partial Q$). This gradient is used in the 4D-Var minimization, but it can become very non-linear as the refractivity profile approaches ducting conditions. However, the gradient limit does not appear to be the major factor on the positive (o-b) biases over oceans in the 3-4 km vertical interval. An additional experiment was performed for December 2014, where this limit was increased from (-)0.75 N units m^{-1} to (-)0.95 N units m^{-1}. Figure 1.10 shows the profile of the bending angle (o-b) biases for the rectangular region defined by the corners (north, south, east, west = 0, -30, 0, -30), for the period December 1-31, 2014. This region was chosen because it has a strong positive bending angle bias in the 3-4 km interval (Figure 1.9). Relaxing the maximum gradient reduces the largest bias near 3.3 km slightly, but the main pattern remains. This may suggest that the bias in the 3-4 km interval originates from a dry bias in the ECMWF short-range forecasts in this region, rather than a measurement or forward model limitation. This is of interest to the ROM SAF, because the ECMWF short-range forecasts are used as background information in the operational refractivity 1D-Var retrievals, and this would potentially bias the moisture retrievals. A difficulty will be validating the 1D-Var humidity retrievals over the ocean against reliable observations, given that all other satellite radiances are currently bias corrected to the NWP model. It is also noteworthy that we do not attempt to either forward model or assimilate bending angles below a ducting layer in the short-range forecast with the ROPP observation operators. We do not impose a similar restriction for the refractivity 1D-Var computation, but this should be given some consideration.

Impact of 2D operator

The technical implementation of the 2D operator used in the CTL experiment is described in Healy (2014). The 2D approach can be compared with results produced with the ROPP 1D operator. The use of a 2D operator should reduce forward model errors, because it makes use of the horizontal refractive index gradient information provided by the short-range fore-

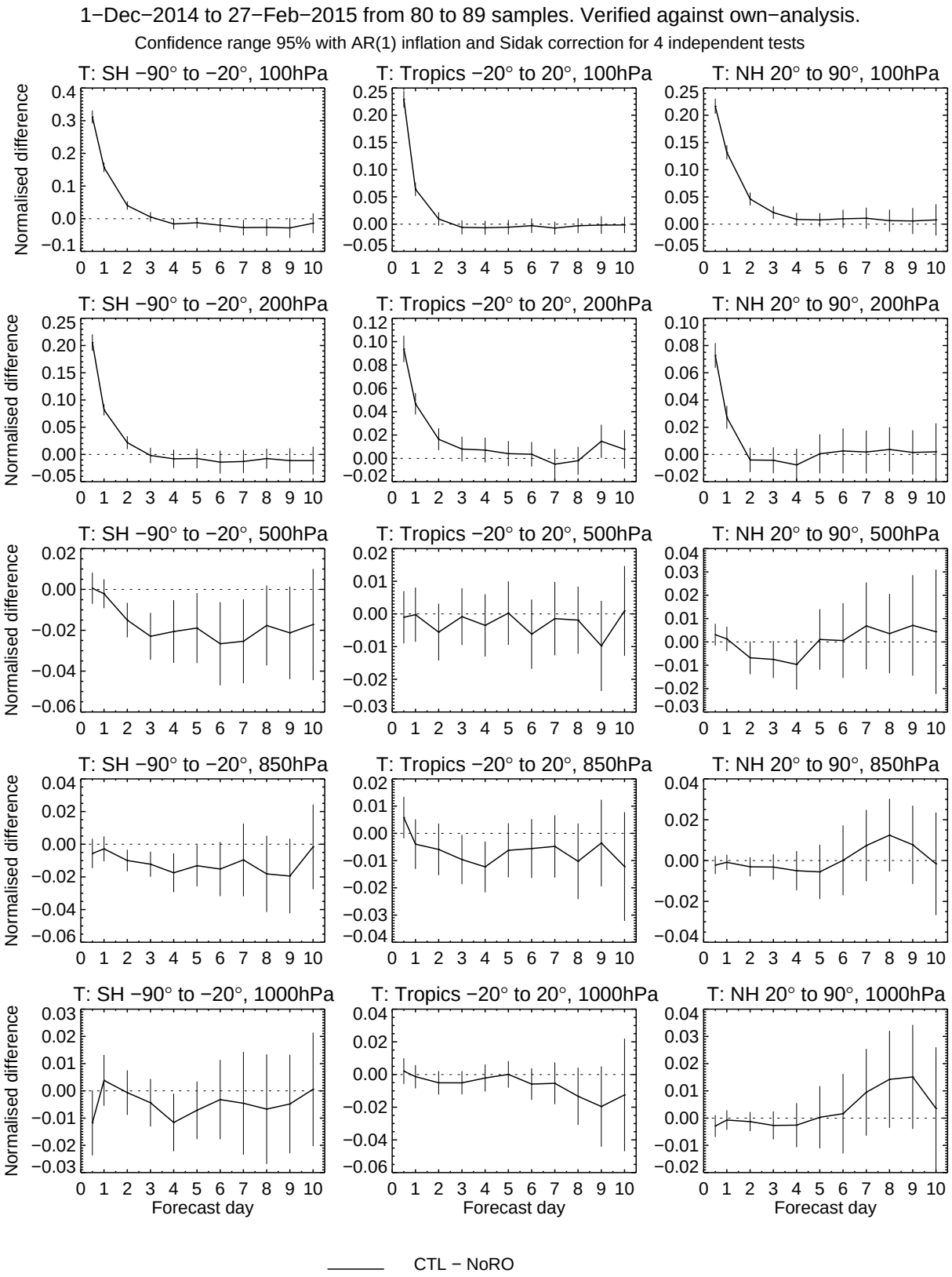

Figure 1.1: The fractional reduction in the standard deviation of the temperature forecast errors on a set of fixed tropospheric and stratospheric pressure levels, for the southern hemisphere, tropics and northern hemisphere. This compares the CTL and NoRO experiments, and a value below the zero line indicates that the GPS-RO data is reducing the forecast errors. The error bars denote the 95 % confidence interval.

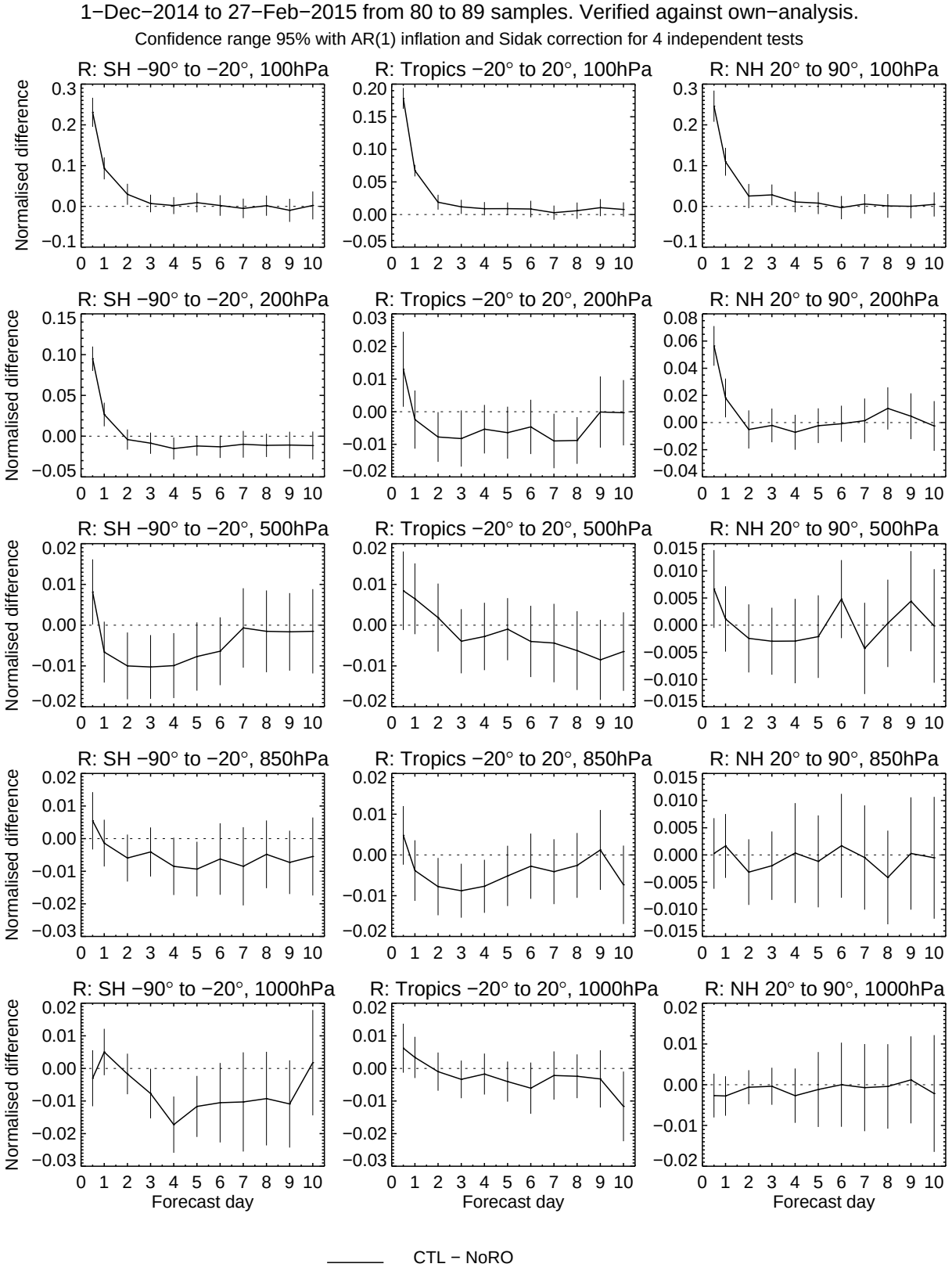

Figure 1.2: As Figure 1.1 but showing the impact of the GPS-RO data on the relative humidity forecast errors.

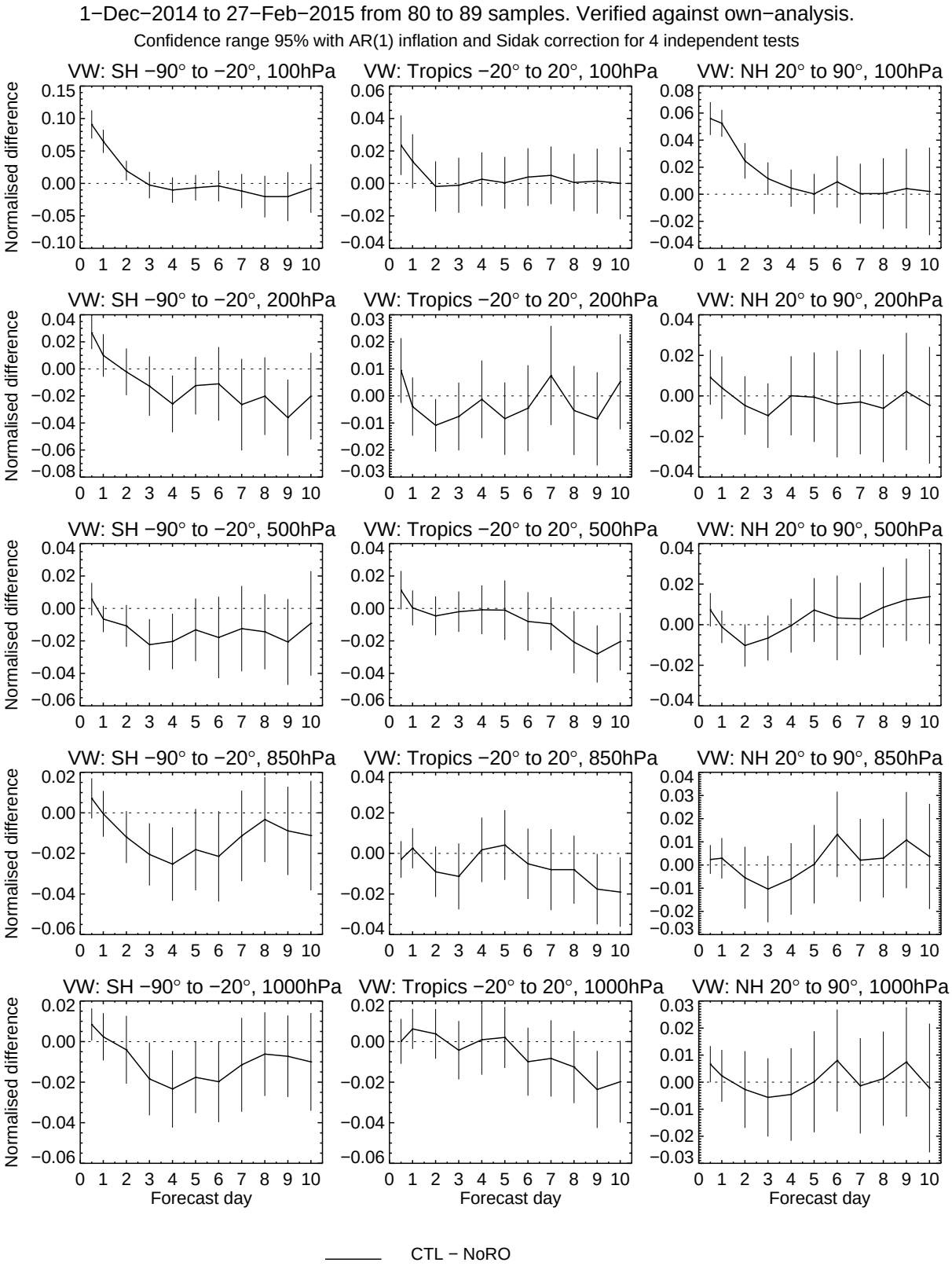

Figure 1.3: As Figure 1.1 but showing the impact of the GPS-RO data on the vector wind forecast errors.

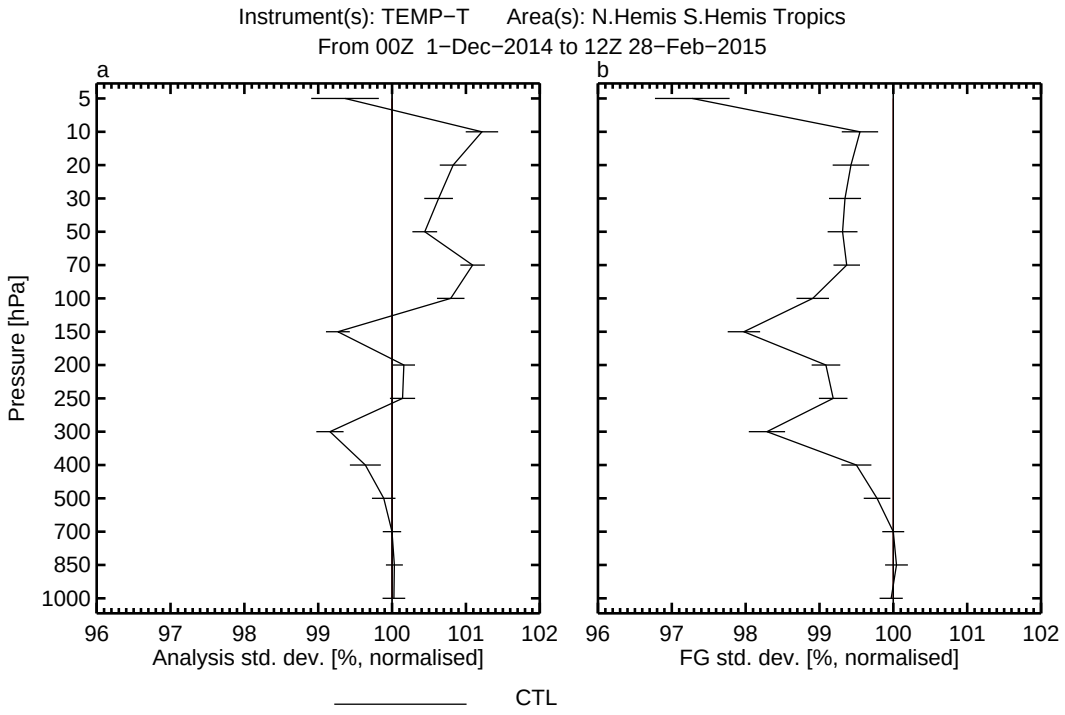

Figure 1.4: The globally averaged percentage change in the standard deviation of the radiosonde temperature departure statistics. The left panel (a) shows the change in the (observation minus analysis) standard deviations and right panel (b) shows the change in the (observation minus background) standard deviations.

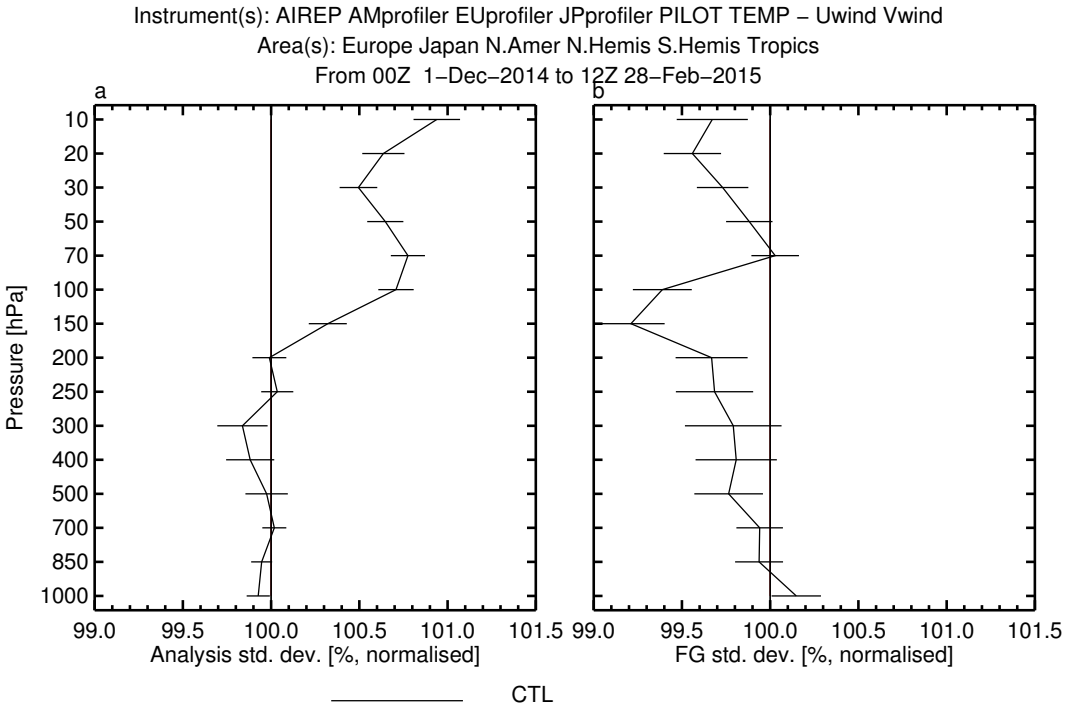

Figure 1.5: As Figure 1.4, but showing the globally averaged percentage change in the standard deviation of the vector wind departure statistics.

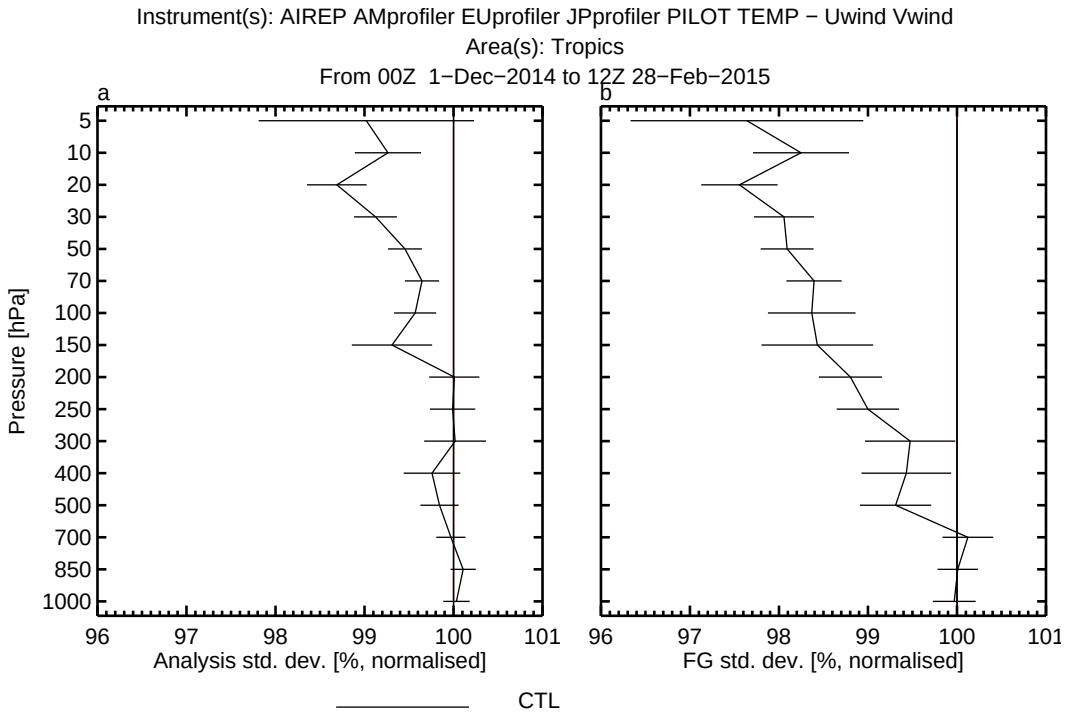

Figure 1.6: As Figure 1.4, but showing the percentage change in the standard deviation of the vector wind departure statistics in the tropics.

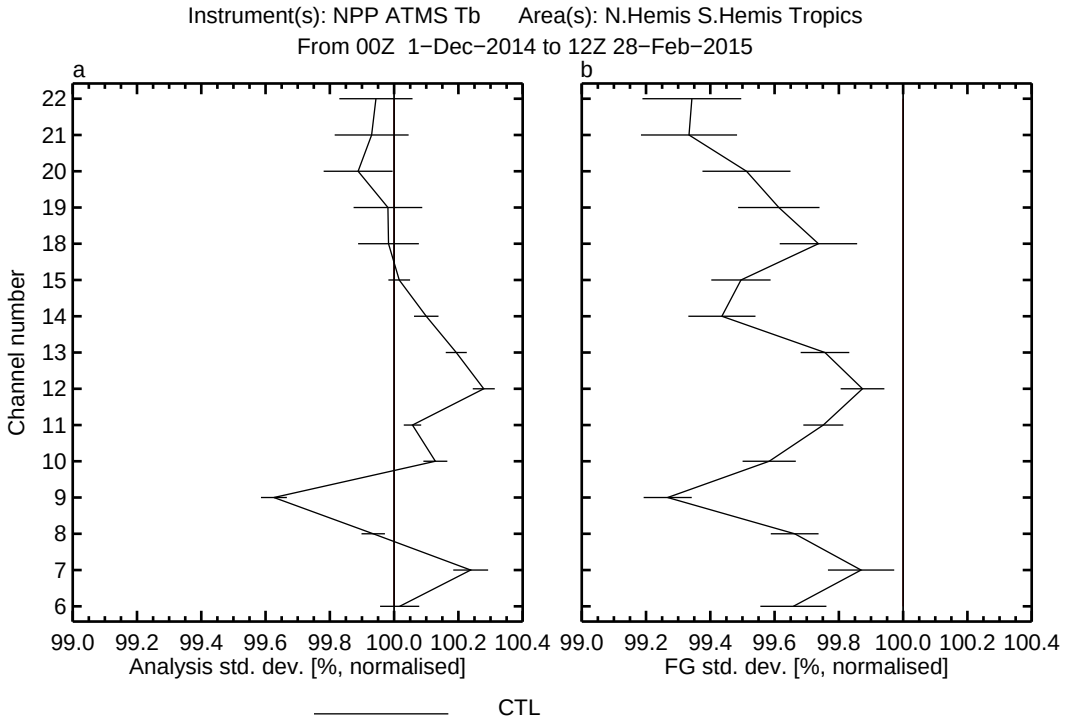

Figure 1.7: As Figure 1.4, but showing the globally averaged percentage change in the standard deviation of the ATMS radiance departure statistics.

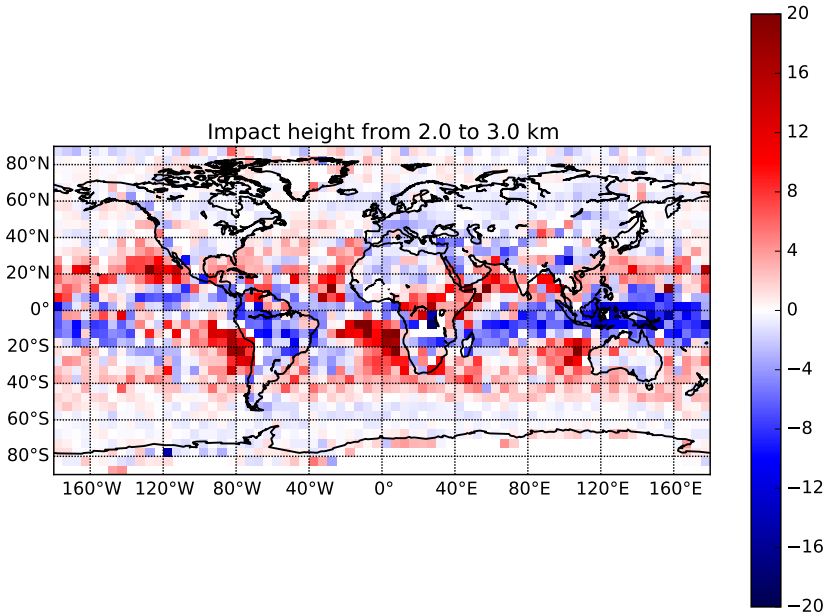

Figure 1.8: The spatial map of the mean (o-b)/b bending angle departures (%) in the 2-3 km impact height interval.

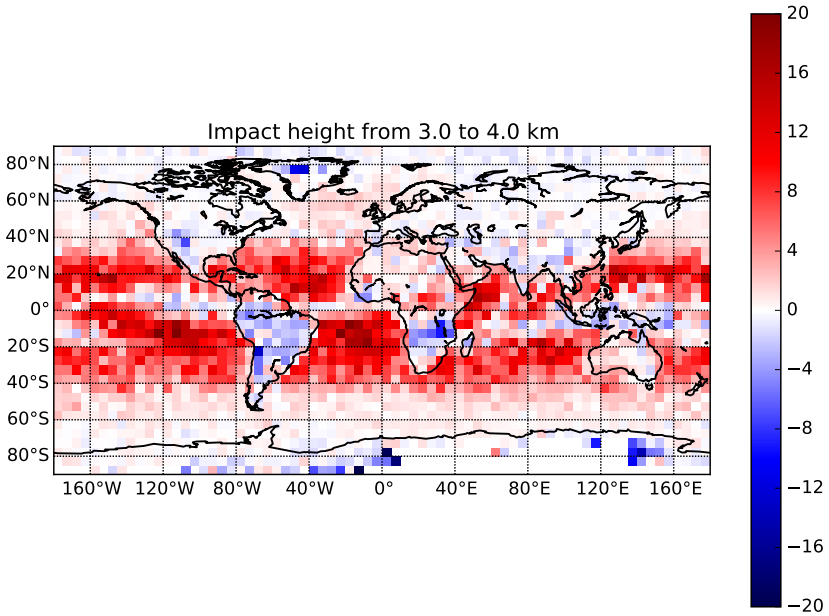

Figure 1.9: The spatial map of the mean (o-b)/b bending angle departures (%) in the 3-4 km impact height interval.

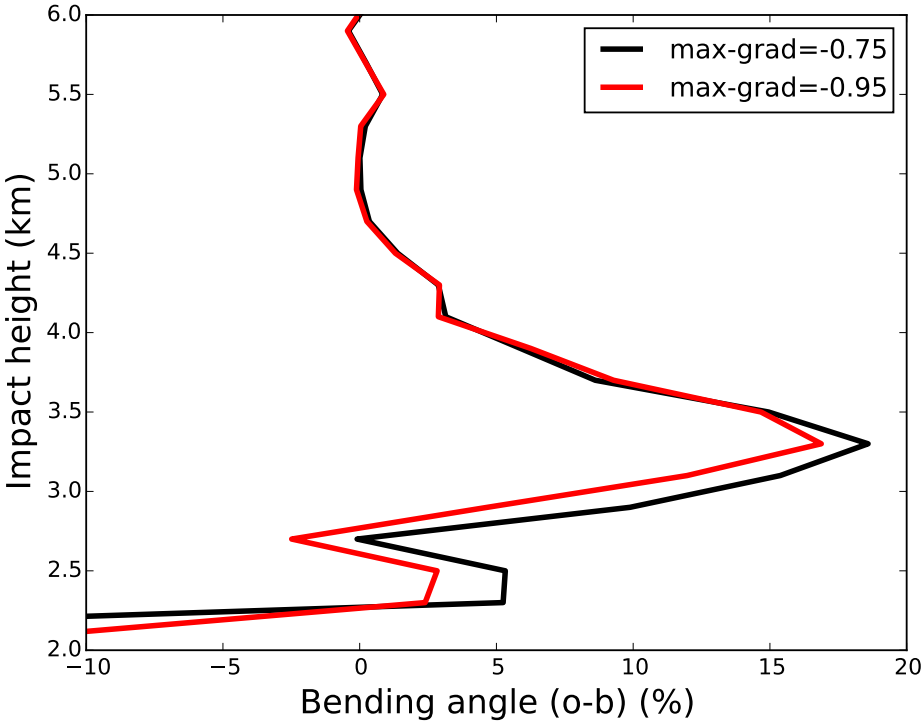

Figure 1.10: The sensitivity of the (o-b) biases to the maximum gradient used in the forward model. The rectangular area is defined by the corners (north,south,east,west=(0,-30,0,-30)). The black line is the from the CTL experiment and the red line is from an experiment where the maximum gradient used in the observation operator is increased from (-) 0.75 N units m^{-1} to (-) 0.95 N units m^{-1}, meaning the forward can produce larger bending angles.

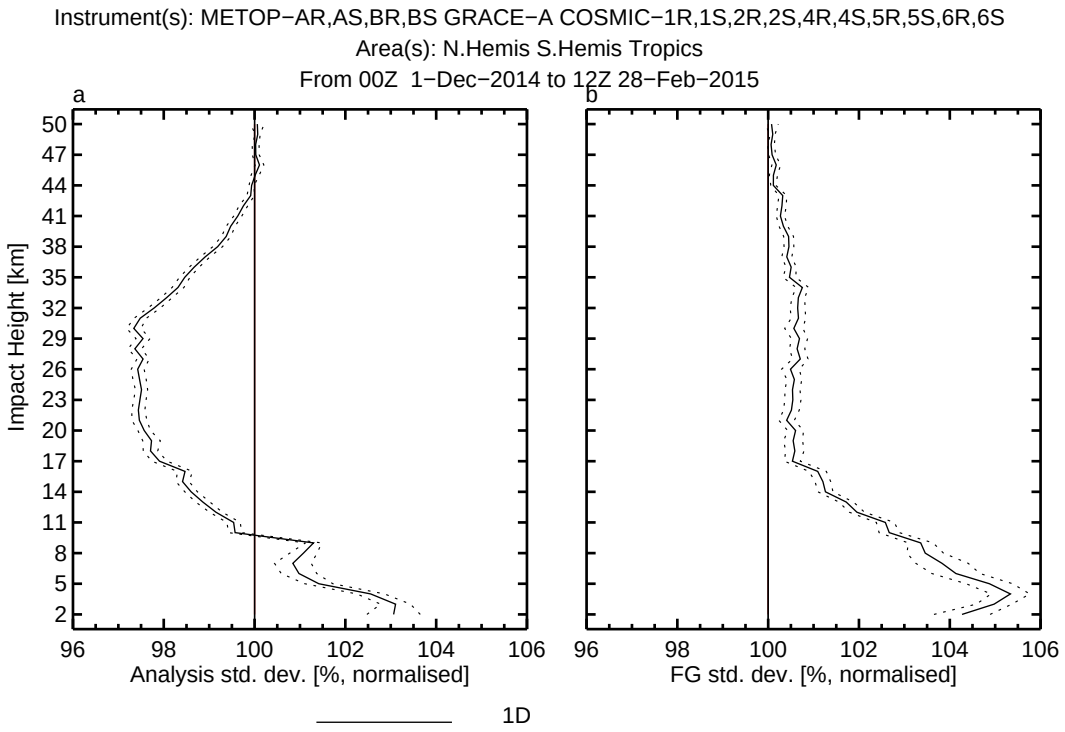

Figure 1.11: The globally averaged change in the standard deviation of the GPS-RO departure statistics comparing the 1D operator and the 2D operator used in the CTL experiment. Values greater than 100 % indicate that the 1D operator is degrading the fit to observations.

cast. The 1D versus 2D, globally averaged statistics are shown in Figure 1.11. As expected, we see the largest improvements in the troposphere ($\sim$ 5 %), where the horizontal gradients are largest, but the (o-b) improvements are statistically significant up to $\sim$ 40 km. There is a degradation in the analysis fit with the 2D operator, but this may be a result of the 2D operator making use of horizontal gradient information that it does not subsequently modify during the assimilation process. In addition, it should be noted that these 1D vs 2D (o-a) differences are relatively small, when compared to the difference between the (o-b) and (o-a) values in both experiments.

In general, the forecast impact of the 2D operator in the short- and medium-range is quite small. For example, the temperature forecast error statistics are shown in Fig 1.12. There is some improvement in the temperatures at 850 hPa in the southern hemisphere with the 2D operator for day 1-3, but generally the results are neutral. Similar results are also found for geopotential height, vector wind and relative humidity. Nevertheless, we feel that the inclusion of the 2D operator is justified since it clearly is a more physically realistic representation of the observation, and it reduces forward model errors.

Sensitivity to assumed observation error statistics

Recent estimates of the bending angle error statistics computed by the ROM SAF (Healy 2016), have indicated that the assumed standard deviation values (σ_o) in the troposphere could be too conservative, although it is should be noted that vertical error correlations are

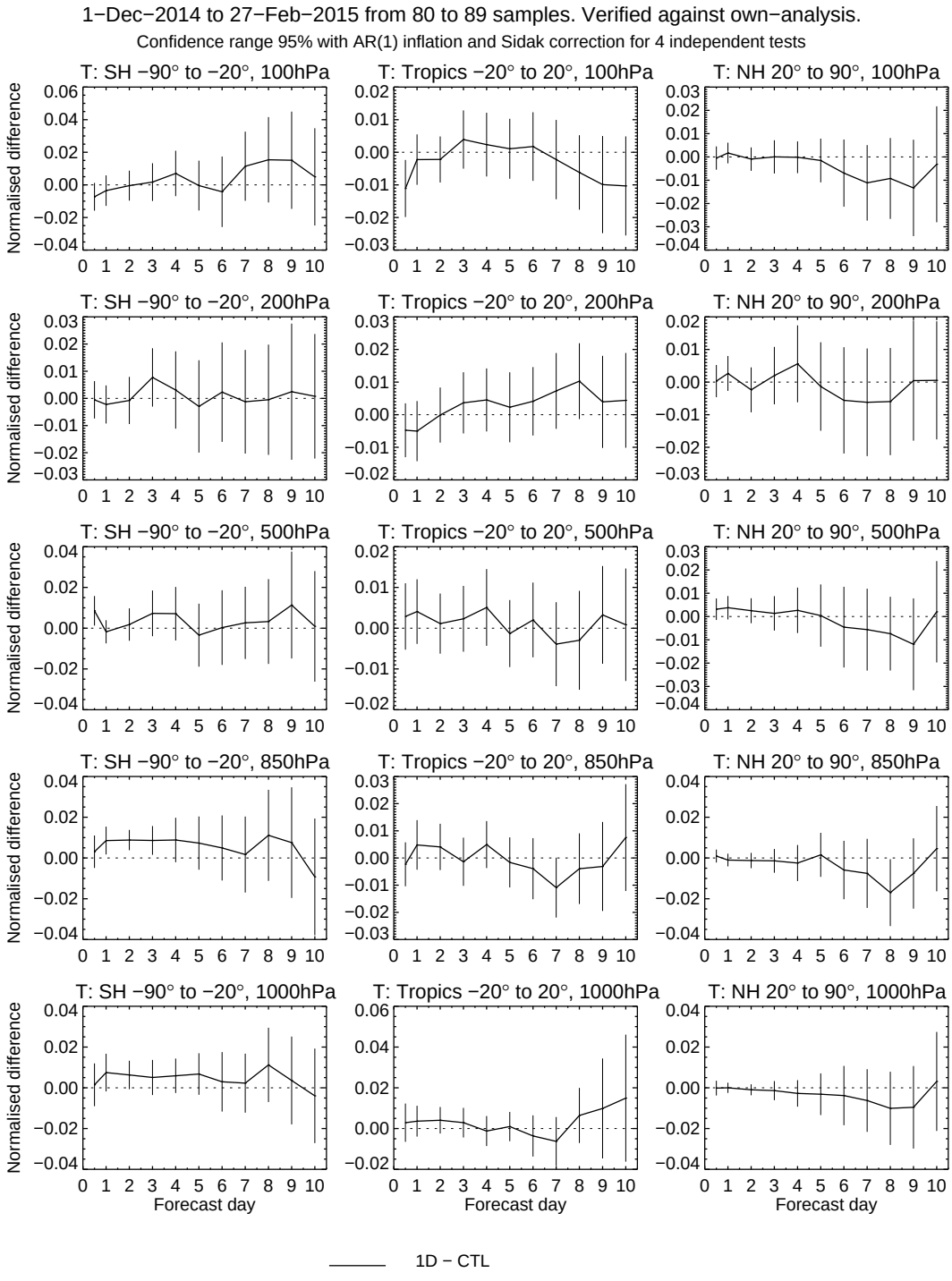

Figure 1.12: The standard deviation of the temperature forecast errors for the 1D operator compared with the CTL experiment. Below the zero line indicates the 1D operator is producing superior forecast error statistics.

ignored at ECMWF when assimilating GPS-RO. We have tested the sensitivity of the forecast results to the assumed GPS-RO error statistics in the troposphere by reducing the assumed errors (HIWT) and increasing them (LOWT). The forecast scores are surprisingly robust to this change, as illustrated in Figure 1.13 for the temperature forecast error statistics, directly comparing the HIWT and LOWT experiments. Values below the zero line indicate that the HIWT experiment is producing better forecast error statistics than the LOWT experiment. There is a degradation in the HIWT results for the temperature at 500 hPa in the southern hemisphere at day-1, but nothing at longer-range. This degradation is most probably caused by larger increments in the HIWT experiment. These sensitivity results suggest that a simple scaling of the assumed tropospheric error statistic model will not produce any significant improvement in forecast performance. However, further investigation of error statistics that vary with latitude, similar to those used at the Met office, should be undertaken.

We find a greater sensitivity to changing the assumed GPS-RO observation error statistics in the stratosphere, particularly in the short-range forecast fits to other observation types. The experiment 43R1 includes both an increase in the assumed error statistics above 10 km, from 1 $\%$ to 1.25 $\%$, and a tightening of the quality control (QC), so that GPS-RO (o-b) departures greater than 6.25 times the assumed observation error (σ_o) are rejected. For comparison, in the CTL experiment this first guess rejection threshold is $\sim 11 \times \sigma_o$, and it has been used operationally at ECMWF since 2006. The increase in the assumed error statistics was initially suggested by Cristina Lupu at ECMWF (Personal Communication), based on adjoint sensitivity calculations, and it is already operational at ECMWF. The change in the QC will be tested for operational implementation soon. Figure 1.14 shows the change in the radiosonde temperature departure statistics between the 43R1 and CTL experiments. Reducing the weight given to the GPS-RO observations allows the analysis to fit other observations more closely in the stratosphere, so the improvements in the (o-a) departures are reasonable. More importantly, this change reduces the (o-b) departures by $\sim$ 0.3 $\%$ above 100 hPa, meaning the short-range forecasts are more consistent with the radiosonde temperatures. This improvement is primarily a result of the change in the assumed observation error statistics, rather than the tightening of the QC. It is slightly smaller than the CTL versus NoRO improvement shown in Figure 1.4, which is $\sim$ 0.5 $\%$ between 100 - 10 hPa, but it is nevertheless clearly significant.

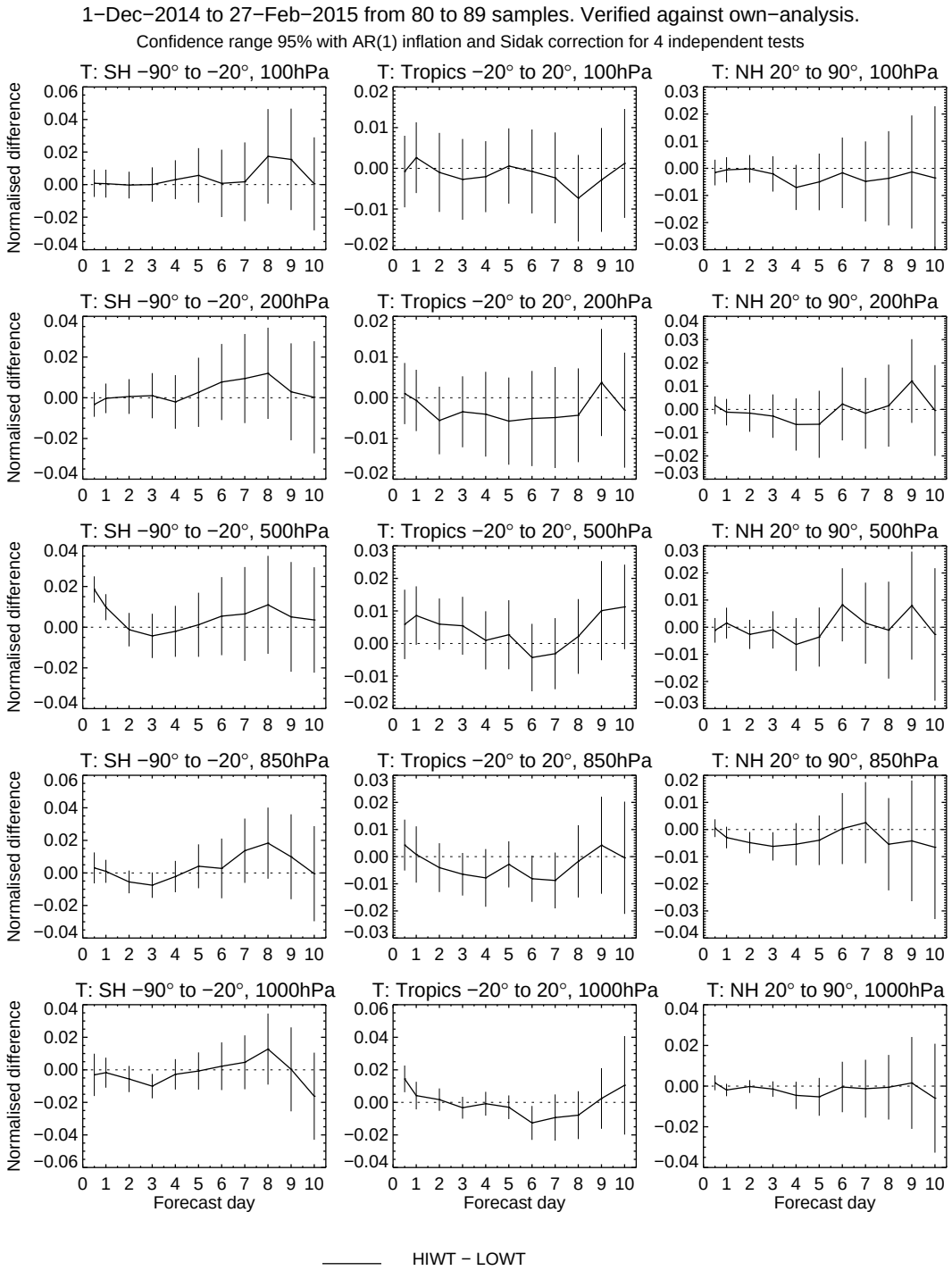

Figure 1.13: The change in the standard deviation of the temperature forecast errors for the HIWT and LOWT experiments. Below the zero line indicates that the HIWT system is producing superior forecast error statistics.

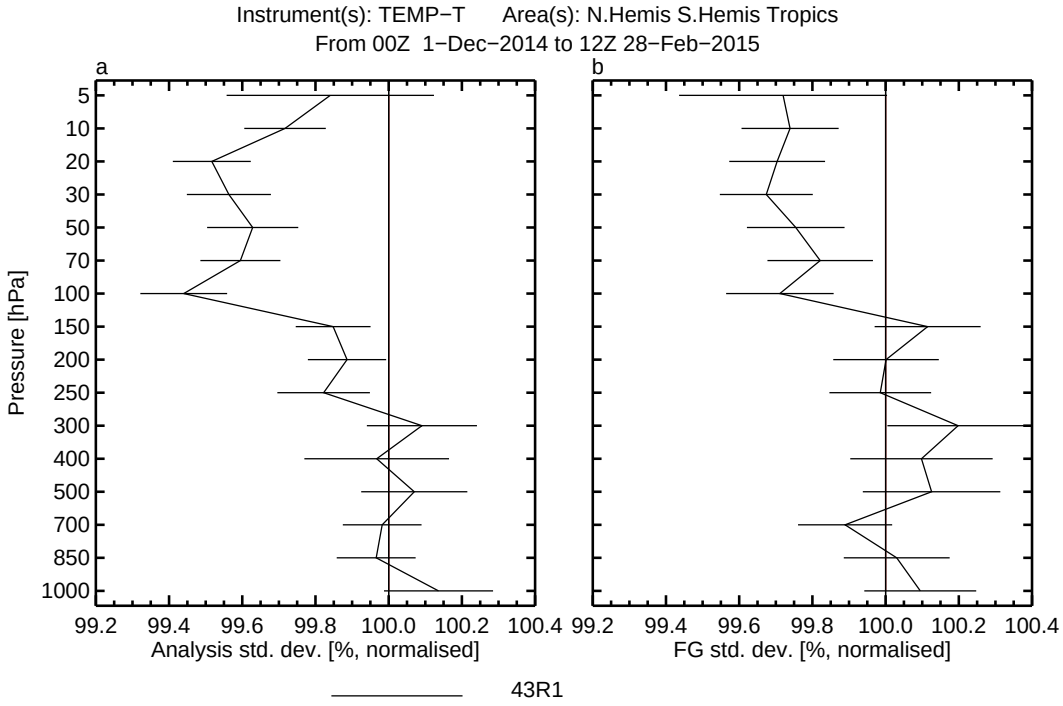

Figure 1.14: The globally averaged change in the standard deviation of the radiosonde temperature departure statistics for the a) (o-a) and b) (o-b) departures. Values below 100 % indicate that the 43R1 departure statistics are better than the CTL values.

2 Summary and Future Work

A series of forecast impact experiments with GPS-RO measurements have been performed. Although the largest GPS-RO forecast impact is still on the upper-tropospheric and lower/mid stratospheric temperature values, we see some improvements in lower-tropospheric relative humidity and vector wind errors in the southern hemisphere, which is encouraging. In addition, the improvement in, for example, the ATMS radiance departures for tropospheric humidity channels also suggests that GPS-RO is providing useful humidity information. One factor that may limit the GPS-RO impact on humidity is biases in the lower troposphere. The mean bending angle departure maps (Figure 1.8 and 1.9) could indicate that the ECMWF model biases are limiting the potential impact of the GPS-RO measurements. In fact, given that all other satellite data is bias corrected to the NWP model, bending angle climatologies in the lower troposphere could become a useful tool for model developers, particularly for investigating humidity biases over oceans. However, some caution still is required because we know that the lower-troposphere is also where GPS-RO errors increase significantly. Nevertheless, demonstrating the use GPS-RO climatologies for lower tropospheric applications should be an area of future work for the ROM SAF. In addition, spatial maps of the bending angle statistics, similar to Figure 1.8 and 1.9, could be added to the ROM SAF monitoring plots. It would be particularly interesting for users to be able to compare the equivalent spatial maps generated with both the Met Office and ECMWF NWP systems, to enable model issues to be highlighted and considered when assessing the measurement characteristics. This will also be important for the operational ROM SAF 1D-Var calculations, because the ECMWF short-range forecasts provide the background information for the computation.

Although forward modelling with the 2D operator clearly improves the GPS-RO departure statistics, the subsequent additional impact on NWP forecasts is relatively small when compared to the assimilation with a 1D operator. There is a positive impact on southern hemisphere temperatures at 850 hPa (Figure 1.12), but more generally the other results are essentially neutral. It is possible that the 2D operator is more beneficial in operational systems, because they run at higher horizontal resolution than the experiments performed here. However, this has not been tested in this study. We will continue to develop the ROM SAF 2D operator to improve the assimilation in the troposphere. To date, attempting to model the impact parameter variation along the ray-path has not proved beneficial. It is likely that a better understanding of the impact of horizontal gradients on wave optics retrievals, such as the full spectrum inversion (Jensen *et al.*, 2003), is required before further improvements of the 2D operator are introduced.

The main forecast impact results do not appear to be very sensitive to variations on the assumed GPS-RO error statistics in the troposphere. However, increasing the assumed errors above 10 km from 1 % to 1.25 % does improve short-range forecast departure statistics in the stratosphere, including radiosonde temperatures (Figure 1.14). The revised GPS-RO bending angle error statistics used at ECMWF should be mapped to refractivity space and be compared with those used for the operational refractivity 1D-Var calculations.

Finally, one unexpected and interesting result is the positive GPS-RO impact on tropical

winds in the stratosphere (Figure 1.6). The mechanism for this improvement is not obvious and this result requires further investigation.

Acknowledgments

I would like to acknowledge useful conversations with Chris Burrows during the course of this study.

Bibliography

[1] Ao, C. O., T. K. Meehan, G. A. Hajj, A. J. Mannucci, and G. Beyerle, 2003: Lower troposphere refractivity bias in GPS occultation retrievals. *J. Geophys. Res.*, **108**, doi:10.1029/2002JD003216.

[2] Bormann, N., A. Fouilloux, and W. Bell, 2013: Evaluation and assimilation of ATMS data in the ECMWF system. *J. Geophys. Res.*, **118**, 12,970–12,980, doi: 10.1002/2013JD020325.

[3] Culverwell, I. D., H. W. Lewis, D. Offiler, C. Marquardt, and C. P. Burrows, 2015: The radio occultation processing package, ROPP. *Atmos. Meas. Tech.*, **8**, 1887–1899, doi:10.5194/amt–8–1887–2015.

[4] Geer, A., 2015: Significance in changes in medium-range forecast scores. Technical Memorandum 766, ECMWF, Reading, UK.

[5] Healy, S. B., 2013: Surface pressure information retrieved from GPS radio occultation measurements. *Q. J. R. Meteorol. Soc.*, **139**, 2108–2118. doi: 10.1002/qj.2090.

[6] Healy, S. B., 2014: Implementation of the ROPP two-dimensional bending angle observation operator in an NWP system. Technical memorandum 19, ROM SAF, http://www.romsaf.org/rsr.php.

[7] Healy, S. B., 2016: Estimates of GNSS radio occultation bending angle and refractivity error statistics. ROM SAF Science Report 26, ROM SAF, http://www.romsaf.org/rsr.php.

[8] Jensen, A., M. Lohmann, H.-H. Benzon, and A. Nielsen, 2003: Full Spectrum Inversion of radio occultation signals. *Radio Sci.*, **38**, 1040, doi:10.1029/2002RS002763.

ROM SAF (and GRAS SAF) Reports

SAF/GRAS/METO/REP/GSR/001	Mono-dimensional thinning for GPS Radio Occulation
SAF/GRAS/METO/REP/GSR/002	Geodesy calculations in ROPP
SAF/GRAS/METO/REP/GSR/003	ROPP minimiser - minROPP
SAF/GRAS/METO/REP/GSR/004	Error function calculation in ROPP
SAF/GRAS/METO/REP/GSR/005	Refractivity calculations in ROPP
SAF/GRAS/METO/REP/GSR/006	Levenberg-Marquardt minimisation in ROPP
SAF/GRAS/METO/REP/GSR/007	Abel integral calculations in ROPP
SAF/GRAS/METO/REP/GSR/008	ROPP thinner algorithm
SAF/GRAS/METO/REP/GSR/009	Refractivity coefficients used in the assimilation of GPS radio occultation measurements
SAF/GRAS/METO/REP/GSR/010	Latitudinal Binning and Area-Weighted Averaging of Irregularly Distributed Radio Occultation Data
SAF/GRAS/METO/REP/GSR/011	ROPP 1dVar validation
SAF/GRAS/METO/REP/GSR/012	Assimilation of Global Positioning System Radio Occultation Data in the ECMWF ERA-Interim Re-analysis
SAF/GRAS/METO/REP/GSR/013	ROPP PP validation
SAF/ROM/METO/REP/RSR/014	A review of the geodesy calculations in ROPP
SAF/ROM/METO/REP/RSR/015	Improvements to the ROPP refractivity and bending angle operators
SAF/ROM/METO/REP/RSR/016	Simplifying EGM96 Undulation calculations in ROPP
SAF/ROM/METO/REP/RSR/017	Simulation of L1 and L2 bending angles with a model ionosphere
SAF/ROM/METO/REP/RSR/018	Single Frequency Radio Occultation Retrievals: Impact on Numerical Weather Prediction
SAF/ROM/METO/REP/RSR/019	Implementation of the ROPP two-dimensional bending angle observation operator in an NWP system
SAF/ROM/METO/REP/RSR/020	Interpolation artefact in ECMWF monthly standard deviation plots
SAF/ROM/METO/REP/RSR/021	5th ROM SAF User Workshop on Applications of GPS radio occultation measurements
SAF/ROM/METO/REP/RSR/022	The use of the GPS radio occultation reflection flag for NWP applications
SAF/ROM/METO/REP/RSR/023	Assessment of a potential reflection flag product
SAF/ROM/METO/REP/RSR/024	The calculation of planetary boundary layer heights in ROPP
SAF/ROM/METO/REP/RSR/025	Survey on user requirements for ionospheric products
SAF/ROM/METO/REP/RSR/026	Estimates of GNSS radio occultation bending angle and refractivity error statistics

ROM SAF Reports are accessible via the ROM SAF website: http://www.romsaf.org